Physics – Uspekhi **53** (10) 1053 – 1065 (2010)

METHODOLOGICAL NOTES PACS numbers: 52.27.Lw, 52.65.Yy, 61.72.J–, 64.70.D

On melting criteria for complex plasma

B A Klumov

DOI: 10.3367/UFNe.0180.201010e.1095

Contents

Abstract. The present paper considers melting criteria for a plasma crystal discovered in dust plasma in 1994. Separate discussions are devoted to three-dimensional (3D) and two-dimensional (2D) systems. In the 3D case, melting criteria are derived based on the properties of local order in a system of microparticles. The order parameters are constructed from the cumulative distributions of the microparticle probability distributions as functions of various rotational invariants. The melting criteria proposed are constructed using *static* information on microparticle positions: a few snapshots of the system that allow for the determination of particle coordinates are enough to determine the phase state of the system. It is shown that criteria obtained in this way describe well the melting and premelting of 3D complex plasmas. In 2D systems, a system of microparticles interacting via a screened Coulomb (i.e., Debye–Hückel or Yukawa) potential is considered as an example, using molecular dynamics simulations. A number of new order parameters characterizing the melting of 2D complex plasmas are proposed. The order parameters and melting criteria proposed for 2D and 3D complex plasmas can be applied to other systems as well.

1. Introduction

In recent years there has been greatly increased interest in the processes occurring in plasma containing microparticles. Such plasma is commonly referred to as complex or dusty plasma. A general review of complex plasma (CP) can be found in, for example, a *Physics–Uspekhi* paper [1]. The interest in dusty plasma is due, on the one hand, to its large natural abundance. On the other hand, given that current laboratory experiments allow each individual microparticle to be fully resolved for its behavior, a kinetic level description of the properties of the ensemble of dusty particles becomes possible. This makes dusty plasma an attractive tool for fundamental research in, among others, such areas as phase transitions [2–4], understanding the nature of hydrodynamic instabilities [5], and the properties of crystallization waves [6, 7].

Knowing particle trajectories offers an additional advantage when studying melting and crystallization of strongly coupled systems, in particular, when constructing melting criteria (which is exactly the subject of this article). Although the melting criteria we discuss here are derived for complex (dusty) plasma, they have, in our view, a much broader range of application and can be used to determine the phase state of a wide variety of systems, including metallic glasses and melts, colloidal and biological crystals, granular media, and so forth.

It should be noted that with current technology it takes relatively short time, $\tau_s \simeq 1-10$ s, to determine the x, y, z coordinates of $N \sim 10^5$ microparticles in a complex (dusty) plasma [8–10]. In the most common procedure, the dust cloud is scanned by a laser beam which is preliminary expanded into a light sheet with a required thickness on the order of the mean interparticle distance in the system. The time this process takes depends on the movement mechanics of the laser-equipped video camera, and to date has exceeded the characteristic times of phase transformations (melting, crystallization) that occur in a CP. However, if τ_s is reduced by only an order of magnitude, which there is every reason to hope is a near-term possibility, it will be possible to determine not only the positions but also the trajectories of the microparticles in space, thus enabling the experimental investigation of the *kinetics* of the melting and crystallization of such systems.

As far as two-dimensional CP and colloidal 2D systems are concerned, this question was resolved long ago: high-resolution video cameras make it possible to determine the trajectories of $N \sim 10^3-10^4$ particles in a system, and so experimentally monitor processes (in particular, phase transformations like melting and crystallization) in the system.

The knowledge of individual microparticle trajectories in a three- and two-dimensional, strongly coupled complex

B A Klumov Max Planck Institute for Extraterrestrial Physics, Postfach 1312, Giessenbechstrasse 85748, Garching 85741, Germany
Tel. (49 89) 30000 33 96. Fax (49 89) 30000 35 69
E-mail: klumov@mpe.mpg.de
Institute of Thermophysics of Extreme States, Joint Institute for High Temperatures, Russian Academy of Sciences, ul. Izhorskaya 13/19, 125412 Moscow, Russian Federation
Tel. (7-495) 485 81 77
E-mail: klumov@ihed.ras.ru

Received 27 April 2010, revised 22 June 2010
Uspekhi Fizicheskikh Nauk **180** (10) 1095 – 1108 (2010)
DOI: 10.3367/UFNr.0180.201010e.1095
Translated by E G Strel'chenko; edited by A Radzig

plasmas allows the experimental verification of dynamic melting criteria (such as, for instance, the well-known Lindemann criterion which states that a system starts melting when the ratio of the root-mean-square displacement of a particle to the average interparticle separation exceeds a certain threshold value [1]).

It should also be noted that the experimental verification of the Lindemann criterion for 3D systems is still a very challenging task, so it is a problem of considerable current interest to develop phase transformation (in particular, melting) criteria based on the *statical* characteristics of the system of atoms (or microparticles) — for example, a snapshot of particle coordinates. For a CP, as has been noted above, such a snapshot is obtained by laser beam scanning of a dust cloud (details of a typical experiment can be found in, for example, Refs [1, 8]).

Under laboratory conditions, complex (dusty) plasma is traditionally obtained by introducing microparticles into a weakly ionized, low-temperature, reduced-pressure, inert gas-discharge plasma. The recombination of electrons and ions on microparticle surfaces causes a rapid charging of the particles, the charge depending on particle size and plasma parameters; as an example, for a commonly used radio-frequency (rf) argon discharge, a particle of size $a \simeq 1$ μm acquires a negative charge $Z_d/e \sim 10^3$, where e is the elementary charge. With such a large microparticle charge, the dusty component is often strongly coupled (coupling parameter Γ is defined as the ratio of the potential energy of interaction between neighboring particles to their temperature: $\Gamma = Z_d^2/(\Delta T_d) > 1$, where Δ is the average interparticle distance, and T_d is the microparticle temperature). Dusty subsystem can exist in a wide variety of phase states, showing its worth as a gas, liquid, or crystal. The crystalline state of the dusty component of a CP (plasma crystal) was discovered experimentally in 1994 [13, 14] after having been predicted theoretically in 1986 [15].

Because electrons diffuse rapidly to the walls of a discharge chamber, the central part of the gas discharge is charged positively, thus making a potential well (confinement) for negatively charged microparticles. The confining potential has a near-parabolic profile [16]. In the near-electrode region of the discharge, the electric field grows much faster compared with the center, so that the confinement can be described here as a rigid elastic wall (hard wall confinement). The pair interaction between microparticles can usually be modeled by a screened Coulomb (Debye–Hückel or Yukawa) potential; the presence of a neutral gas in plasma causes particles to slow down (neutral drag). Thus, dust particles can form highly ordered structures in the discharge, often referred to as plasma crystals. Notice that due to the presence of controlled damping, which obviously is absent in atomic systems, dusty structures in a CP can be formed into (or manipulated between) various phase states.

Recent experiments aboard the International Space Station (ISS) with three-dimensional confined complex plasmas [2] [17–19] are the first detailed observation of crystallization and melting processes in a three-dimensional plasma crystal. The results obtained and the subsequent molecular dynamics simulation of a 3D complex plasma have made it possible to formulate melting criteria for such systems, which are discussed, in particular, in Section 2.

Section 3 uses the example of a system of microparticles interacting via a screened Coulomb potential to examine the melting of a two-dimensional (2D) complex plasma.

2. Melting of a three-dimensional complex plasma: experiment and simulation

Figure 1 displays several snapshots (scans) from a three-dimensional plasma crystal recently observed aboard the ISS (details of the experiment can be found in Ref. [17]; the structural properties of this CP are discussed in Refs [18, 19]). The snapshots demonstrate how a dusty subsystem evolves as the control parameter — the low-frequency field applied to the lower electrode — varies. The color of microparticles or, in the printed version (PV), the degree of darkening is determined by local order (the local order parameter we use here, q_6, will be discussed later). The crystalline (solid) phase is shown by light (red and orange) color, whereas the weakly ordered (liquid or glassy) phase is shown by dark (blue and light green) color, respectively.

The insets depict the way the major CP parameters vary with plasma evolution aboard the ISS. Inset (a) shows the average interparticle distance Δ in a system of microparticles (red line *1*) and the control parameter (green line *2*) as functions of time (the snapshot number). The amplitude of the low-frequency electric field first increased step-by-step to a certain level and then, again step-by-step, decreased to the initial level. The best plasma crystal was observed for the maximum field amplitude. Notice that the hysteresis in the parameter Δ (the final value Δ_{fin} differs significantly from the initial value Δ_0 at the same magnitudes of the field) is evidence that the system of microparticles possesses memory, which is likely due to the effect of the electric field on the confinement region. [3]

Inset (b) presents the time dependence of the parameter Π_m, which characterizes the phase state of the system and is defined from the pair correlation function $g(r)$ [20] as follows:

$$\Pi_m = \frac{g^{max}}{g^{min}}\,, \tag{1}$$

where $g(r)^{max}$ and $g(r)^{min}$ are the first maximum and the first nonzero minimum of the pair correlation function, respectively; $g(r)$ is defined as

$$g(r) = \frac{L^3}{N^2}\left\langle \sum_i^N \sum_{j\neq i}^N \delta(\mathbf{r} - \mathbf{r}_{ij}) \right\rangle\,, \tag{2}$$

where N/L^3 is the density of microparticles in the system, and r_{ij} is the separation between particles i and j. For particles interacting via a Lennard-Jones potential $\phi(r) \propto (\sigma/r)^{12} - (\sigma/r)^6$, it was found that the system melts as $\Pi_m < \Pi_{LJ}^{cr}$,

[1] For two-dimensional systems, the Lindemann criterion is modified to be determined from the relative root-mean-square displacement of nearest neighbors: the trajectories of the nearest neighbors diverge on melting [11, 12].

[2] To obtain a uniform plasma crystal, it is highly desirable to reduce the influence of the gravitational force, so such experiments are usually performed on board spacecraft, under microgravity conditions.

[3] A possible mechanism for the hysteresis is the microparticle charge decrease (and, hence, the decrease in the coupling parameter Γ) upon compression of the system (confinement domain) due to a strengthening of a low-frequency field (an increase in the control parameter), which results in the melting of the CP. The melting of the CP, in turn, changes the conditions in the confinement domain; the difference between the characteristic time scales of melting (upon compressing the dusty subsystem) and crystallization (upon strengthening the field) determine the observed effect.

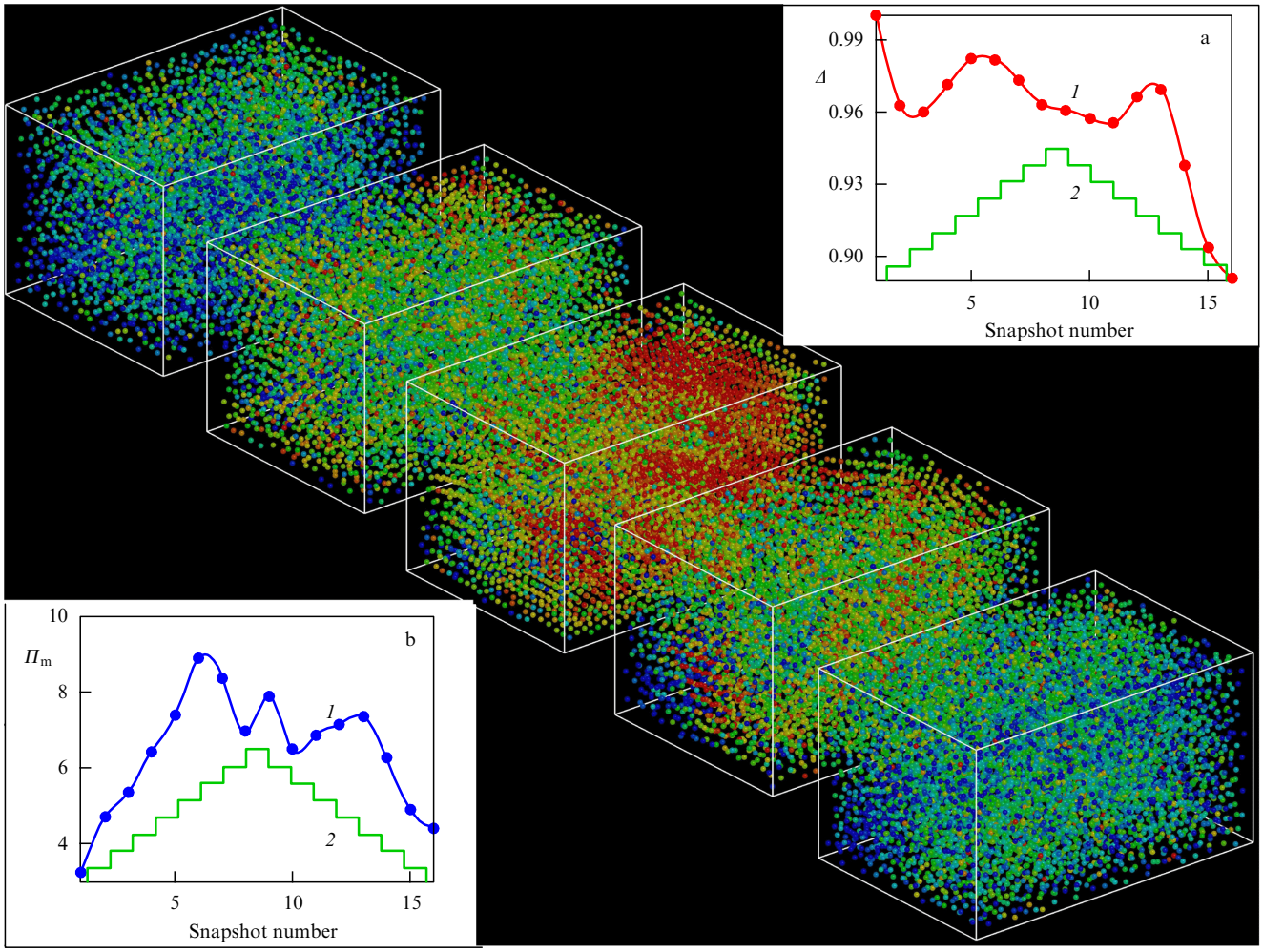

Figure 1. (Color online.) Evolution of a plasma crystal obtained aboard the ISS (the initial state of the system of microparticles is shown in the upper left corner, and the final, in the lower right). Five snapshots of the plasma crystal are presented, which show how the crystal evolves under the action of the control parameter, a low-frequency electric field applied to one of the electrodes. Color or (in the printed version, or PV) the degree of darkening of microparticles depends on the quantity determining local order, viz. the rotational invariant q_6 (see the text for the definition). The solid phase has an orange and red (the brightest in PV) colors ($q_6 \geqslant 0.45$); the weakly ordered liquid (glassy) phase has a blue and light green (dark in PV) colors ($q_6 \leqslant 0.4$). Inset (a) demonstrates the dependence on time (the snapshot number) of the average interparticle distance Δ (red line *1*) and the control parameter (green line *2*). Inset (b) shows the evolution of the melting criterion $\Pi_\mathrm{m} = g^{\max}/g^{\min}$ as determined from the pair correlation function $g(r)$ (blue line *1*); for convenience, as in inset (a), the time dependence of the field is also given (*2*). The behavior of the parameters Π_m and q_6 is evidence of the crystallization of the system of microparticles as the field increases, and of its subsequent melting as the field decreases. The field dependence of the interparticle separation Δ and the hysteresis in the behavior of Δ point to memory effects in the system of microparticles.

whereas for $\Pi_\mathrm{m} > \Pi^{\mathrm{cr}}_{\mathrm{LJ}}$ it resides in a crystalline state, where $\Pi^{\mathrm{cr}}_{\mathrm{LJ}} \approx 5$.

The value of the parameter Π^{cr} depends on the interaction potential between microparticles; however, an increase in Π_m implies increased order in the system (as does the increase in q_6). The way the parameters Π_m and q_6 behave as a plasma crystal evolves points to the crystallization and subsequent melting of the system of microparticles. Notice that the melting criterion Π_m, simple though it is, requires knowing the spatial coordinates of the particles (atoms). We shall show later that with this knowledge much more detailed melting criteria can be derived, based on how local order changes in the crystal–liquid transition.

Local order in a system of microparticles is usually determined applying the local rotational invariants method proposed in Ref. [21]. In this method, one starts by determining $N_\mathrm{nb}(i)$ nearest neighbors for each ith particle. Knowing the vectors $\mathbf{r}_{ij}$ connecting the ith particle with its nearest neighbors ($j = 1, \ldots, N_\mathrm{nb}$) determines the local orientation parameter $q_{lm}(i)$ for each particle:

$$q_{lm}(i) = \frac{1}{N_\mathrm{nb}(i)} \sum_{j=1}^{N_\mathrm{nb}(i)} Y_{lm}(\theta_j, \phi_j)\,, \tag{3}$$

where $Y_{lm}(\theta, \phi)$ are spherical harmonics, and θ_j, ϕ_j are the angular coordinates of the jth particle, determined by the vector $\mathbf{r}_{ij}$. Using the values of $q_{lm}(i)$, which are coordinate system specific (and thus of no use for determining local orientation order), the rotational invariants of rank l of the second, $q_l(i)$, and third, $w_l(i)$, order can be calculated for each microparticle, giving

$$q_l(i) = \left(\frac{4\pi}{2l+1} \sum_{m=-l}^{m=l} \left| q_{lm}(i) \right|^2 \right)^{1/2}, \tag{4}$$

$$w_l(i) = \sum_{m_1, m_2, m_3} \begin{pmatrix} l & l & l \\ m_1 & m_2 & m_3 \end{pmatrix} q_{lm_1}(i) q_{lm_2}(i) q_{lm_3}(i), \tag{5}$$

where

$$\begin{pmatrix} l & l & l \\ m_1 & m_2 & m_3 \end{pmatrix}$$

are the Wigner 3*j*-symbols; the summation in the last equation is carried out over all those indices $m_i = -l, \ldots, l$ for which $(m_1 + m_2 + m_3) = 0$. Since the publication of Ref. [21], this method has been widely used in condensed matter physics for determining the phase state of various systems.

An important point to note is that each lattice type has its own unique set of orientation order parameters (rotational invariants) q_l and w_l. Therefore, a solid-state structure obtained in an experiment or by simulation can be determined by comparing the q_l and w_l values calculated for each particle with the $q_l^{\rm id}$ and $w_l^{\rm id}$ values known for perfect lattices (which means determining local order in the system).

Crystal structure identification usually relies on the use of the rotational invariants of the second (q_4, q_6) and the third (w_4, w_6) orders, which can be calculated quite easily for perfect crystals. For example, for face-centered cubic (fcc) and hexagonal close packed (hcp) crystal lattices, as well as for the icosahedral (ico) phase, the number of the nearest neighbors for each particle is $N_{\rm nb} = 12$, and the respective invariants are

1) for fcc: $q_4^{\rm fcc} = 0.1909$, $q_6^{\rm fcc} = 0.5745$, $w_4^{\rm fcc} = -0.1593$ $w_6^{\rm fcc} = -0.01316$;

2) for hcp: $q_4^{\rm hcp} = 0.0972$, $q_6^{\rm hcp} = 0.4847$, $w_4^{\rm hcp} = 0.1341$, $w_6^{\rm hcp} = = -0.01244$;

3) for ico: $q_4^{\rm ico} = 0$, $q_6^{\rm ico} = 0.6633$, $w_4^{\rm ico} = -0.1593$, $w_6^{\rm ico} = -0.1697$.

The high values of the parameter $q_6^{\rm cr}$ for all crystal lattice types considered allow both the initial stage of crystallization (nucleation) in various systems (see, for example, Ref. [22]) and the structural properties of glassy [10] and crystallizing [23] CP to be studied. Notice that for a weakly correlated system of particles (gas or liquid) the average rotational invariant $\langle q_6 \rangle \simeq N_{\rm nb}^{-1/2}$ (for example, for $N_{\rm nb} = 12$ the average value of $\langle q_6 \rangle \approx 0.29$), which is much less than the value of q_6 characteristic of ordered systems ($q_6^{\rm cr} \geqslant 0.45$).

For a body-centered cubic lattice, the number of the nearest neighbors is $N_{\rm nb} = 8$, and the rotational invariants are $q_4^{\rm bcc} = 0.5092$, $q_6^{\rm bcc} = 0.6285$, $w_4^{\rm bcc} = -0.1593$, $w_6^{\rm bcc} = 0.1316$. In determining clusters with the bcc type symmetry, the position of the second shell of nearest neighbors comprising 6 particles, which is at a small distance of $(2/\sqrt{3} - 1)\Delta \simeq 0.15\Delta$ from the first shell of nearest neighbors, is often important. In this case, $N_{\rm nb} = 14$ and $q_4^{\rm bcc} = 0.0363$, $q_6^{\rm bcc} = 0.510$, $w_4^{\rm bcc} = 0.1593$, $w_6^{\rm bcc} = 0.01316$.

Figure 2 displays the microparticle distribution in the $q_4 - q_6$ plane for the two CP states considered above: (a) a melt (glassy state), and (b) a plasma crystal. The insets show the spatial position of the microparticles (as in Fig. 1, particles are color-coded according to the value of q_6). It is clearly seen that the plasma crystal consists primarily of hcp-like particles and partially of the fcc phase. It can be shown [16] that the plasma crystal in question also contains some amount of the bcc phase. A melt is, from the point of view of local order, a weakly ordered system of particles with an average value of $q_6 \simeq 0.4$. Note that this value greatly exceeds the value for the liquid phase ($q_6 \simeq 0.29$), so that this phase state can be properly called glassy (as far as a statical characteristic — local order — is concerned). Clearly, the dynamics of the change of local order is a more accurate means to determine

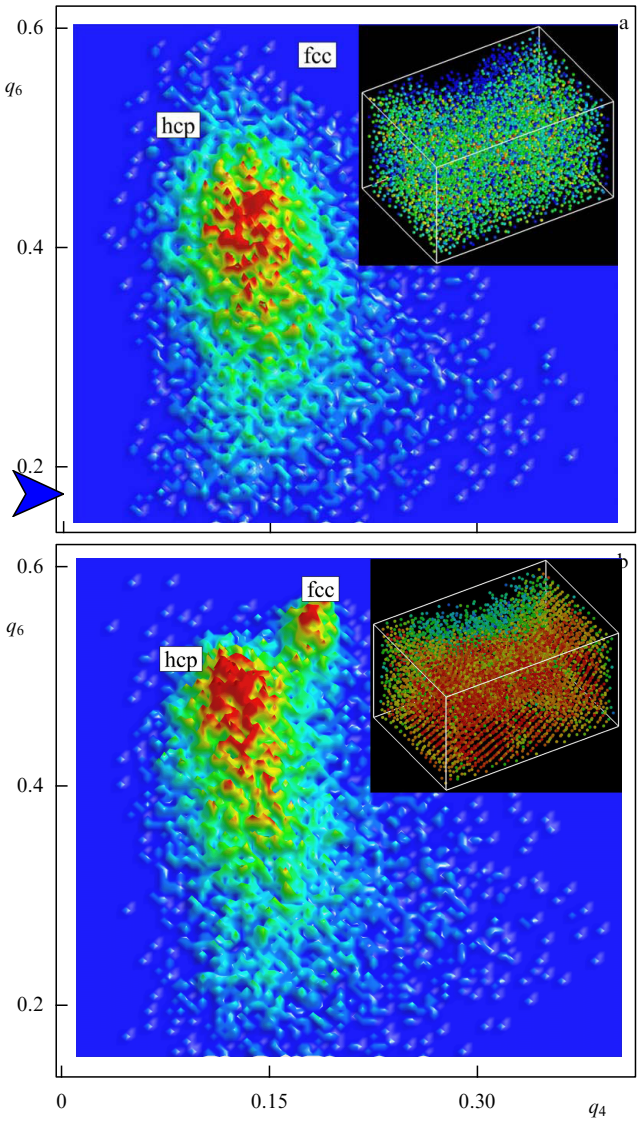

Figure 2. (Color online.) Structural properties of a plasma crystal obtained aboard the ISS for various melting stages. Shown is the distribution of microparticles in the plane $q_4 - q_6$ for two states of a complex plasma: (a) melt (glassy phase), and (b) plasma crystal. The values of the local order parameters q_4 and q_6 were calculated using 12 nearest neighbors for each microparticle in order to determine the hcp, fcc, and ico phases in the system under consideration. The insets show the spatial position of microparticles, color-coded according to the value of q_6. It is clearly seen that the plasma crystal consists primarily of hcp-like particles, with a considerable mixture of the fcc phase. The melt (glassy state) is, from a local order point of view, a weakly ordered system of particles with the average value of $q_6 \simeq 0.4$, which greatly exceeds the average quantity $\langle q_6 \rangle$ for a disordered system ($q_6 \simeq 0.29$).

the type of the phase state and the character of phase transformations in a system of microparticles.

Unfortunately, space experiments with CP, whose results have been used above, produced only a limited amount of dynamics information: as little as twenty snapshots (scans) of the plasma crystal. These snapshots contain the 3D coordinates of microparticles and indicate how CP evolves under the action of the control parameter (which in this case is a low-frequency electric field applied to one of the electrodes). The crystallization and melting stages of a plasma crystal each contain about 10 frames which, while very informative about the structural changes in the ISS complex plasma, are clearly

insufficient for a detailed local order analysis. Therefore, the discussion below will rely on molecular dynamics (MD) simulation results obtained for a system of charged microparticles interacting via a screened Coulomb potential (Yukawa system). Notice that this simulation reproduces remarkably well the data on the local order variation in the ISS CP in the experiment under consideration [18, 19].

Our MD calculations will use the screened Coulomb (Debye–Hückel or Yukawa) potential [4]

$$\phi(r) = \frac{Z_d}{r} \exp\left(-\frac{r}{\lambda_D}\right), \tag{6}$$

(with r being the interparticle distance, and λ_D the characteristic screening length) to simulate the pair interaction between the microparticles (from now on we shall call such a system a Yukawa system for the sake of brevity). This means that the coupling parameter for this dusty subsystem is defined as

$$\Gamma \equiv \frac{Z_d^2}{T_d \Delta} \geqslant 1, \tag{7}$$

where T_d is the temperature of the microparticles, and Δ is the average interparticle separation. The structural parameter $\varkappa = \Delta/\lambda_D$ was chosen to be close to that found in experiment. For simplicity, it is assumed that all the particles have the same fixed size $a \approx 1$ μm, and charge $Z_d \approx 3 \times 10^3$. The equations of motion of an individual microparticle have the form

$$m\ddot{\mathbf{r}}_i = -Z_d \nabla \Phi_c - Z_d \sum \nabla \phi - m\gamma \dot{\mathbf{r}}_i + \mathbf{L}_i. \tag{8}$$

The terms on the right-hand side of Eqn (8), along with describing the electrostatic interaction between the particles, describe (a) the deceleration of dust particles in their collisions with neutral atoms and molecules of a buffer gas, (b) the random Langevin force $\mathbf{L}_i$ (thermal noise induced by neutral atoms) which is determined from

$$\langle \mathbf{L}_i(t)\, \mathbf{L}_j(t+\tau) \rangle = 2\gamma m k_B T_g \delta_{ij} \delta(\tau) \tag{9}$$

under the condition of zero average value, $\langle \mathbf{L}_i(t) \rangle = 0$, and (c) the interaction of microparticles with the confinement potential Φ_c.

It is worth noting that equations (8) and (9) describe the so-called Langevin thermostat (because the temperatures of gas and dust particles are compared for long time intervals) which is widely used in the MD simulation of a variety of systems.

The system of equations (8), (9) was solved for $N \simeq 40{,}000$ microparticles randomly distributed at the initial time inside a cube $L \simeq 0.3$ cm in size. Confinement restricts the z positions of microparticles to $-L/2 \leqslant z \leqslant L/2$. The boundary conditions at the sides of the cube were taken to be periodic. The confinement electric field grows exponentially for $z > L/2$ with a characteristic spatial scale $d_w \simeq \Delta/3$, preventing the microparticles from moving distances $l > d_w$ away from the calculation region.

The remaining simulation parameters were chosen close to their experimental values: $\varkappa \simeq 1-3$, buffer gas pressure $p_g \simeq 10-100$ Pa, gas temperature $T_g \sim 100-1000$ K, and microparticle material density $\rho_d \approx 1.5$ g cm^{-3}. Through the action of friction, such a system crystallizes at large times (when $T_d \approx T_g$) with a coupling parameter $\Gamma \sim 10^3 - 10^5$.

[4] As measured in Ref. [16], the interparticle interaction potential in CP is close to the Yukawa potential.

The melting of the MD-simulated plasma crystal was also calculated by molecular dynamics method; in this calculation, the temperature T_g of the Langevin thermostat was increased by a small amount $\delta T_g \ll T_d$, and the subsequent calculation was stopped, when the system evolved into a quasi-equilibrium state with a new temperature $T_g + \delta T_g$.

The evolution of local order during the melting of the Yukawa system is illustrated in Fig. 3, which shows microparticle distributions as functions of orientational order parameters — the rotational invariants of the second (q_4, q_6) and third (w_4, w_6) orders — for different melting stages of a

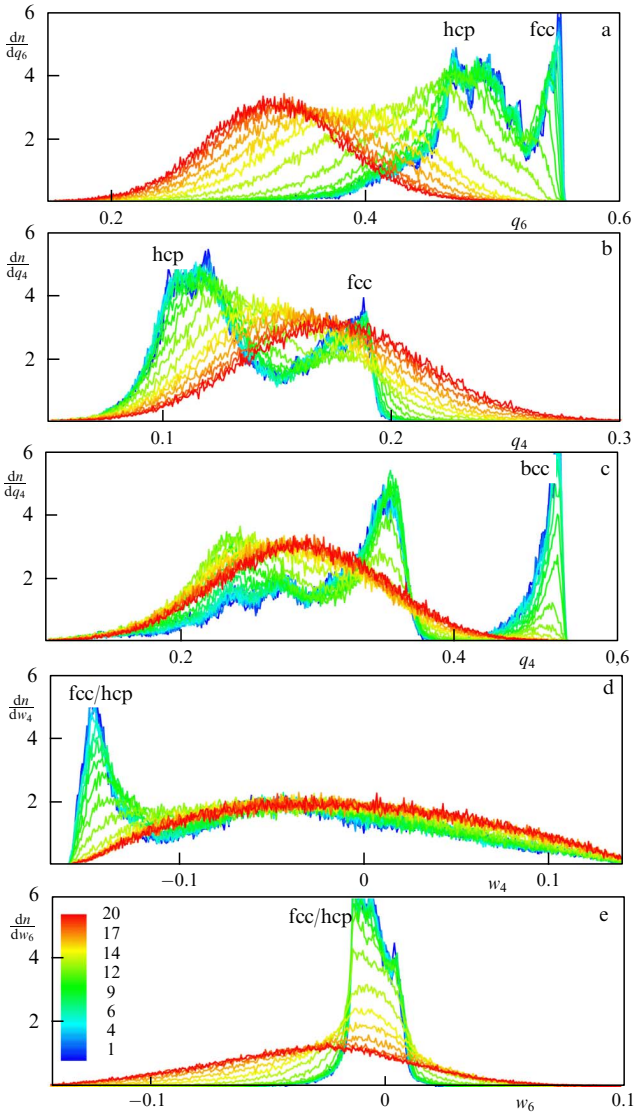

Figure 3. (Color online.) Microparticle probability distributions $dn(q_i)/dq_i$ over the values of rotational invariants q_6 (a), q_4 (b), q_4 (c), w_4 (d), and w_6 (e) at various melting stages for the Yukawa system (for 20 snapshots). Rotational invariants (a, b, d, e) were calculated with 12 nearest neighbors; 8 nearest neighbors were used for (c) (to identify bcc clusters). The color of the curves depends on the temperature of the system, which increases from the first to the 20th snapshot, capturing the stages from the crystalline phase (blue or dark color, the first snapshot) to the final disordered liquid phase (red or light color, 20th snapshot). Indicated are the values of rotational invariants for perfect lattices (hcp, fcc, and bcc). Clearly seen is the premelting stage, namely, a sharp decrease in the number of fcc (a) and bcc (c) particles in the system which still remains solid (most particles exhibit a hcp symmetry).

plasma crystal. The color of the lines varies from blue (dark) for the plasma crystal at the initial stage to red (light) for a dusty liquid as the temperature of the system increases. The peaks on the distribution curves correspond to various crystal lattice types observed in the system of microparticles under study. The simulated plasma crystal mainly consists, as in the space experiments described above, of hcp and fcc phases, with a small portion of bcc-like clusters. Increasing the temperature leads to the premelting of the system — that is, as seen from Fig. 3, fractions such as bcc and fcc disappear, while the solid-state structure of the substance is conserved. Increasing the temperature further leads to the complete melting of the system.

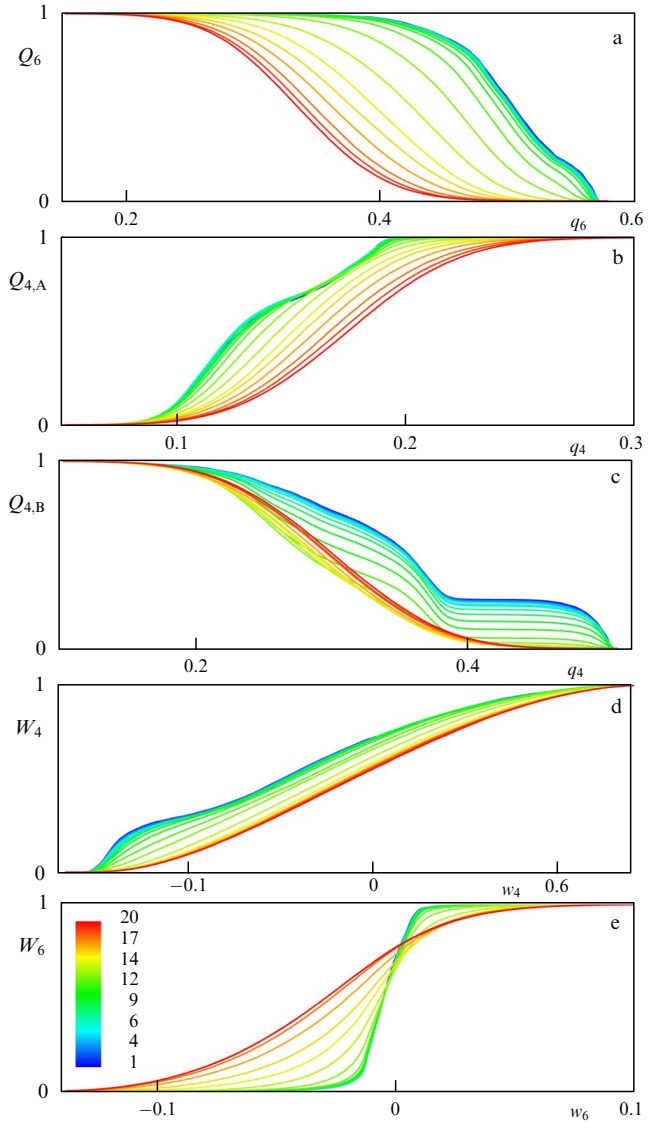

Figure 4. (Color online.) Cumulative distributions for histograms plotted in Fig. 3 as functions of the values of the rotational invariants q_6 (a), q_4 (b), q_4 (c), w_4 (d), and w_6 (e) at different stages of the melting of a three-dimensional Yukawa system. The color of the curve is (as in Fig. 3) determined by the temperature T_d of a system of microparticles, which increases from the first snapshot (blue, the darkest curve, the corresponding state of the system being a highly ordered plasma crystal) to the 20th snapshot (red, the lightest, dusty liquid). The strong dependence of cumulative distributions enables using them for constructing order parameters characterizing the melting and crystallization of a system of microparticles.

Using the cumulative distributions (zero-order cumulants) of the obtained probability distributions, it is a simple matter to construct the order parameters capable of determining the phase state of the system. In particular, for the histogram 3a, which is the distribution of microparticles over the values of the rotational invariant q_6 (which was calculated with $N_{nb} = 12$ to determine the proportion of the hcp and fcc fractions in the system), the zero-order cumulant is naturally defined as

$$Q_6(x) \equiv \frac{1}{N}\int_x^\infty \frac{dn(q_6)}{dq_6}\, dq_6\,, \tag{10}$$

where N is the total number of particles in the system. Clearly, it is given by

$$N = \int_{-\infty}^{\infty} \frac{dn(q_6)}{dq_6}\, dq_6\,,$$

where $dn(q_6)/dq_6$ is the probability distribution in question (Fig. 3a). For such a definition, the cumulant $Q_6(x)$ depends on the relative concentration of fcc clusters in the system.

A possible example of an order parameter is the derivative of the cumulant $Q_6(x)$ at $q_6 = q_6^{fcc}$. From Fig. 4 it is clearly seen that such a derivative is nonzero for a crystalline system and that the melting (or premelting) process — that is, the disappearance of fcc particles — turns it to zero. Using the quantity $Q_6(x)$, one can define one more order parameter, $\Pi_{fcc} = Q_6(x_b)$, where $x_b \simeq 0.55$ (let us recall that for a perfect lattice $q_6^{fcc} = 0.5745$). With this definition, Π_{fcc} stands for the relative fraction of fcc-like particles in the system (the parameter Π_{hcp} for describing the hcp phase is introduced analogously). When the Yukawa system melts, we see that the order parameter Π_{fcc} tends to zero, i.e., the fcc fraction disappears first and, accordingly, this parameter can be utilized for describing the premelting of a system of microparticles. Figure 5 illustrates how the relative concentrations of various phases change as the Yukawa system melts. Premelting stages accompanied by a sharp drop in the density of fcc and bcc clusters are clearly seen in the figure.

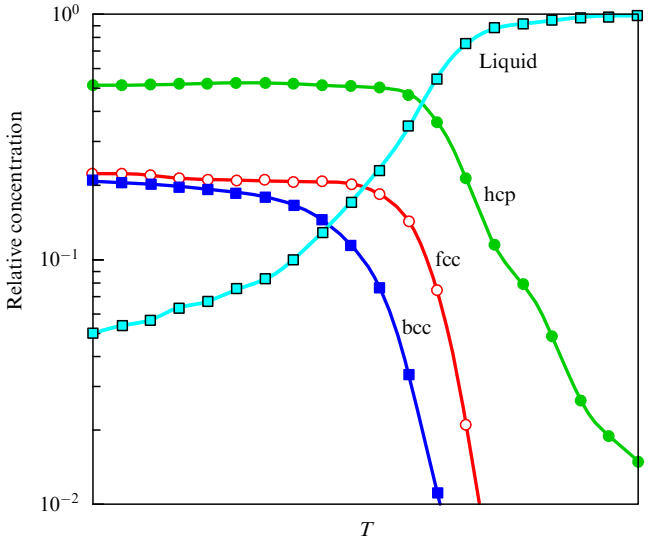

Figure 5. (Color online.) Abundance of different phases in the Yukawa system at different temperatures. Clearly seen is the disappearance of the fcc and bcc phases at the premelting stage of the system.

In the same way, using the cumulative distributions mentioned above provides order parameters for hcp and bcc phases. Note that the idea of employing cumulative distributions is generally that, instead of utilizing relatively complicated probability distribution functions (part of which are shown in Fig. 3 and which often have a number of peaks, making it difficult to rely on their average characteristics such as the often used distribution-averaged invariant $\langle q_6 \rangle$), one introduces smoothed cumulative distributions, much more convenient for constructing order parameters.

Of particular interest in this context is the behavior of the cumulant $W_6(x)$ for microparticle distribution constructed as a function of the parameter $w_6(x)$ (see Fig. 3e):

$$W_6(x) \equiv \frac{1}{N} \int_{-\infty}^{x} \frac{\mathrm{d}n(w_6)}{\mathrm{d}w_6} \, \mathrm{d}w_6 \,. \tag{11}$$

This cumulant proved to be very sensitive to the phase state of a CP, as is readily seen from Fig. 4e. For a highly ordered solid-like CP, the distribution $W_6(x)$ is virtually independent of the parameter Γ. But as soon as the plasma crystal starts melting, a sharp change occurs in $W_6(x)$. Thus, it is possible to construct the melting criterion $\Lambda_{w_6}^{\mathrm{m}}$ for a three-dimensional CP using the cumulative distribution discussed:

$$\Lambda_{w_6}^{\mathrm{m}} \equiv \frac{w_6(W_6 = 0.5)}{w_6^{\mathrm{cr}}(W_6 = 0.5)} \,, \tag{12}$$

where the order parameter is $w_6^{\mathrm{cr}}(W_6 = 0.5) \approx -5 \times 10^{-3}$ and is determined from the value of w_6 under the condition that $W_6 = 0.5$ (at the half height of the cumulative distribution).

With this definition of parameter $\Lambda_{w_6}^{\mathrm{m}}$, the CP starts melting for $\Lambda_{w_6}^{\mathrm{m}} < 3.4$, as is clearly seen in Fig. 6, in which a number of order parameters being discussed are shown as functions of the CP temperature.* For comparison, Fig. 6 also displays the temperature dependence of the parameter Π_{m} (determined from the pair correlation function). It should be noted that corresponding to plasma crystal melting as defined in a new way ($\Lambda_{w_6}^{\mathrm{m}} \approx 3.4$) is the value of $\Pi_{\mathrm{m}} \simeq 4.3$, which is much less than that for the melting of systems with a Lennard-Jones interaction potential. This means, in particular, that the melting criterion Π_{m} is not universal, but rather is interaction-dependent.

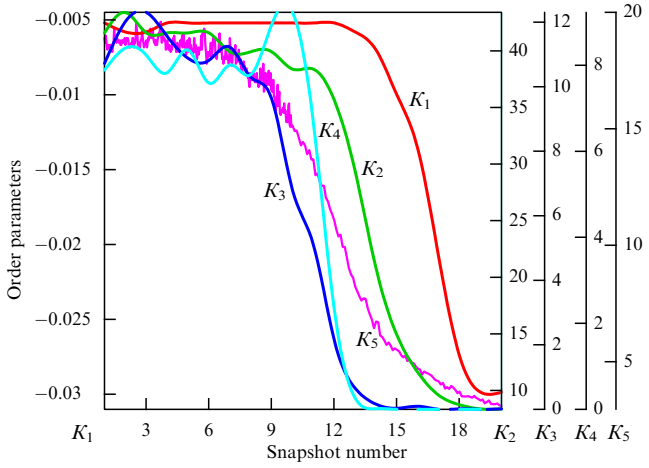

Figure 6. (Color online.) Various order parameters characterizing the premelting and melting of a three-dimensional Yukawa system and constructed from the cumulative distributions shown in Fig. 4 are plotted as a function of the snapshot number (microparticle temperature). Presented are order parameters describing the premelting of the system — the disappearance of fcc (blue line, K_4) and bcc (dark blue line, K_3) phases — and obtained from the distributions (a) and (c) in Fig. 4, respectively. The melting of the hcp phase (obtained from the distribution (a) in Fig. 3) is determined by the order parameter Π_{hcp} (green line, K_2). The purple line (K_5) fits the values of parameter Π_{m} for the same snapshot numbers. Variations of parameter $\Lambda_{w_6}^{\mathrm{m}}$ (obtained from the distribution plotted in Fig. 4e) during the melting of the system are shown by the red line (K_1). Because of its high sensitivity to the phase state of a system, parameter $\Lambda_{w_6}^{\mathrm{m}}$ is usable as a new melting criterion for three-dimensional systems.

Thus, this article suggests new order parameters for describing the melting of a three-dimensional complex plasma, which rely on structural changes (changes in local order) that occur in the system during melting (or freezing). It is to be emphasized that these order parameters are sensitive to changes in the structural properties of a microparticle ensemble and that they incorporate the influence of small phase fractions, for example, fcc and bcc, which allows for describing CP *premelting* as well. It is reasonably believed that the applicability of this approach goes beyond CP.

3. Melting of two-dimensional systems

Since the pioneering studies [24–27], there has been steadily increasing interest in processes occurring in strongly coupled two-dimensional systems. Here is a (not exhaustive) list of physical objects whose properties are strongly sensitive to dimensionality of the system: ultracold atoms (Bose–Einstein condensate) in an optical lattice, with their possible relation to quantum computing [28, 29]; quasi-two-dimensional carbon layers (graphene) [30, 31]; vortex lattices in planar superconductors [32]; electrons on a liquid-helium surface and quasi-two-dimensional colloidal systems [33, 34]; granular media [35], and two-dimensional plasma crystals in CP (a planar layer of microparticles) [36]. Of particular interest is the behavior of such systems near a crystal–liquid phase transition,** where the structural defects of the crystal lattice are well known to be a key factor.

In this section we shall consider the kinetics of structural defects in a two-dimensional (2D) confined complex plasma in a parameter range close to the solid–liquid phase transition and, as in three dimensions, we shall propose a number of new order parameters for characterizing the melting and crystallization of such systems. By defects we mean here all structural defects in a two-dimensional lattice; thus, point defects (disclinations) and pair defects (dislocations) are not assigned to a separate group. The reason is that, as will be shown below, the clusterization of defects, i.e., the distribution of clusters by the number of contained single defects, is one of the major parameters of the solid–liquid transition we are studying. Notice that, experimentally, the solid–liquid phase transition is particularly conveniently studied in colloidal suspensions [37] and in complex (dusty) plasmas [38, 39]. Research on such systems (for example, colloidal and plasma crystals) has generated vast literature (see, for example, Refs [40–45]). Still, the kinetics of defects, mechanisms of their formation, association (agglomeration), and loss

* It is more convenient to use here $w_6^{\mathrm{fcc}} \approx -1.316 \times 10^{-2}$ instead of $w_6^{\mathrm{cr}} \approx -5 \times 10^{-3}$ as in Russian edition; accordingly, melting criterion $\Lambda_{w_6}^{\mathrm{m}}$ also changes proportionally. (*Author's note added in English proof.*)

** Comprehensive studies of 2D melting were performed in Refs [51–53]. (*Author's note added in English proof.*)

during melting (crystallization), and the structural properties of crystallizing 2D systems have been relatively poorly studied.

This is due in part to the fact that both in colloidal systems and two-dimensional CP there is usually only a small number ($N_{\rm exp} \simeq 10^4$) of particles whose trajectories can be fully resolved experimentally (with high-resolution cameras), and so the kinetics of defects is difficult to study. While in a three-dimensional CP the number of microparticles $N_{\rm exp} \simeq 10^4$ is quite sufficient to determine the phase state of a system (see the above example of the ISS plasma crystal), in two dimensions it is not, even when taken into account that the particles whose trajectories are determined constitute only a small fraction of the plasma crystal.

The crystallization process strongly reduces the number of defects (the abundance of defects in a crystallizing plasma crystal usually ranges from a few to a fraction of a percent of the total number of particles). Hence, as of today, experiments with $N_{\rm exp} \simeq 10^4$ microparticles can hardly provide valuable statistical information, for instance, on the size distribution of defect clusters, the orientational properties of crystallites, etc. [5] Such information can, however, be obtained by numerical simulation. In this section, as in considering a three-dimensional plasma crystal in the previous section, we again apply molecular dynamics to the simple example of a Yukawa system to investigate the evolution of a two-dimensional CP in the solid–liquid transition region. It is known (see, for example, Ref. [16]) that the Yukawa potential describes adequately the pairwise interaction between dusty microparticles in CP.

At the initial instant of time, $N = 1 \times 10^6$ microparticles of size $a = 1$ μm and charge $Z_{\rm d} = 3 \times 10^3$ elementary charges are distributed randomly in the simulation region (a square with $L_x = L_y = 2-10$ cm). The remaining parameters of MD simulation are chosen to be close to the experimental values (the structural parameter $\varkappa = \Delta/\lambda_{\rm D} \simeq 1-3$, and the neutral gas pressure determining the deceleration of microparticles is $p \simeq 0.01-1$ Pa). As in the 3D case, the MD method combined with the use of a Langevin thermostat was employed (see, for example, monograph [47]).

The disordered Yukawa system was chosen to be initially in a nearly gaseous state, with a coupling parameter $\Gamma < 1$. After the system of microparticles fairly rapidly thermalizes to a temperature $T_{\rm d}$, the subsequent kinetic processes of defect formation and loss are studied in an isothermal system.

Notice that the initial *post-thermalization* concentration of point defects in the Yukawa system was taken to be superequilibrium, which allowed a detailed study of the kinetics of defect loss (annihilation) in the system during its subsequent evolution. The study considered the two-dimensional and quasi-two-dimensional versions of a crystallizing Yukawa system. In the latter case, simulation was performed for a three-dimensional Yukawa system, but with the variations δz of the third coordinate z suppressed ($\delta z \ll \Delta$) by the vertical confinement. In ground-based experiments with a two-dimensional dusty plasma, the factors that confine microparticles vertically are gravitation and the electric field which strengthens sharply near the electrodes. Because the study revealed no noticeable difference in defect kinetics between the 2D and quasi-2D cases, the results obtained can be extended to a quasi-two-dimensional CP.

It is well known that a strongly coupled ($\Gamma \gg 1$) two-dimensional Yukawa system (plasma crystal) possesses in the ground state a hexagonal crystal lattice, with each microparticle having six nearest neighbors located at the vertices of a regular hexagon. Structural defects here are usually particles with 5 and 7 nearest neighbors (particles with 4 or 8 neighbors are usually present in low concentrations, if at all). Point defects with 5 or 7 neighbors (disclinations) often unite to form a relatively stable dislocation (a pair of defects with 5 and 7 nearest neighbors). The interaction between structural defects causes them, depending on their orientation, either to annihilate (recombine) or to unite to form clusters consisting of point defects. Such clusters can have a significantly larger number of defects ($N \gg 1$) and a rather complex (fractal) structure. The study of the properties of such clusters and their relation to melting (crystallization) is one of the objectives of this article. Notably, the peculiarities of spatial correlations in relation to the solid–liquid phase transition (consecutive destruction of translational and orientational orders in the process of melting) are not discussed here and can be found reviewed in recent literature (see, for example, Ref. [33]).

Shown in Fig. 7 are some essential aspects of how a crystallizing Yukawa system evolves at a specified temperature. The left and right parts of the figure present, from top to bottom, the distribution of defects, local orientational order in the system, and the orientation of domains containing microparticles with 6 neighbors, for the initial and final states of a two-dimensional Yukawa system.[6] We note that the final state of the system is nonequilibrium: the concentration of defects is not yet quasistationary. The nearest neighbors of each microparticle were determined using Delaunay triangulation followed by dividing 2D space by the Voronoi cell method. Local orientational order in the system is defined by the parameter Ψ_6 which for the kth particle has the form

$$\Psi_6(k) \equiv \frac{1}{N_j} \sum_j \exp\left(6i\theta_{jk}\right), \tag{13}$$

where the angle θ_{jk} is determined by the line joining the particles j, k in the fixed coordinate system (the summation is over the nearest neighbors). For the perfect hexagonal lattice (hexagon), one has $|\Psi_6| = 1$. It is clearly seen that the crystallization leads to the formation of a polycrystalline structure consisting of variously oriented crystallites (crystal lattice domains) whose average size increases with time; we note that small crystallites disappear (are absorbed) much faster than large ones. Domain boundaries are usually linear clusters consisting of structural lattice defects. The number of domains $N_{\rm D}$ in such a system is readily estimated from

$$\ln N_{\rm D} \sim \frac{N_{\rm d}}{\sqrt{N}}, \tag{14}$$

where N and $N_{\rm d}$ are the respective numbers of particles and defects in the system.

Simple though it is, this estimate shows that to study the behavior of such crystallites, the number of microparticles in

[5] Adding difficulty to quasi-two-dimensional dusty plasma experiments is the fact that plasma crystal microparticles are kept from flying away by a confinement electric field, which is usually strongly nonuniform (the confinement potential $\phi_{\rm c}$ is nearly parabolic: $\phi_{\rm c} \propto r^2$), and this results in a nonuniform plasma crystal [48].

[6] For a much more detailed presentation of the evolution process, see the computer-animated MD simulation results in the paper's online version at www.ufn.ru.

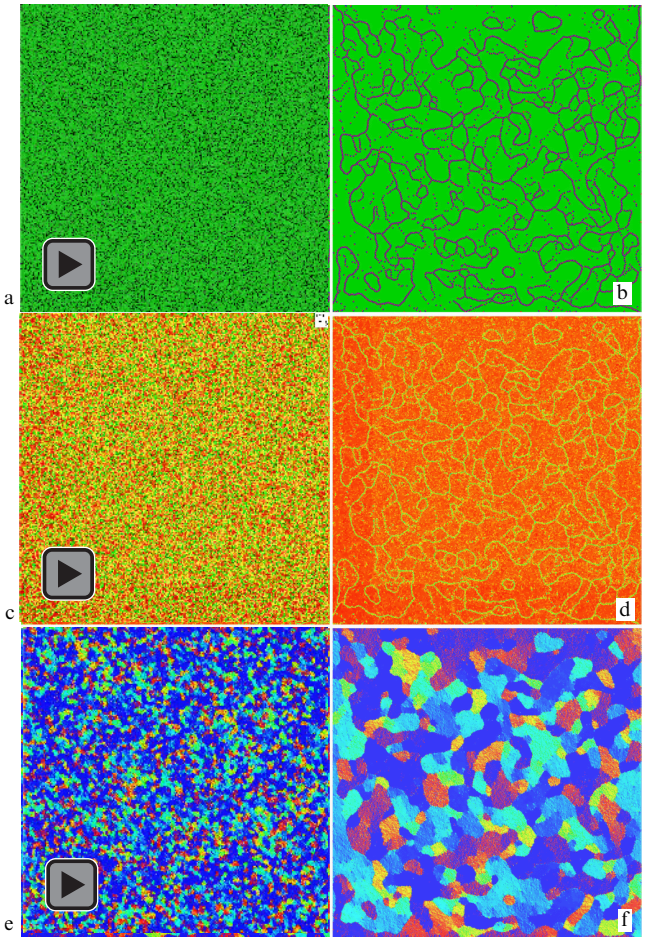

Figure 7. (Color and animation online.) Patterns of crystallizing, isothermal, two-dimensional Yukawa system. Shown are the initial (a, c, e) and final (b, d, f) nonequilibrium (not yet stationary) distributions: of defects (a, b), of the parameter Ψ_6 characterizing local orientational order (c, d), and crystallite orientation (e, f), respectively. Microparticles with 6 neighbors (a, b) are marked by green color (background); structural defects: red (light) color marks particles with 7 or more nearest neighbors (NN), and blue (dark), particles with 5 or fewer NN. Red color (background) for microparticles (c, d) corresponds to the value of $|\Psi_6| \approx 1$, i.e., to nearly perfect hexagonal order in the system, while distortions of orientational order (yellow and green, light-grey in the printed version of the paper) are due to the presence of structural defects. In figures e, f, color variations are determined by the orientation of the local hexagon in each crystallite. Boundaries between neighboring crystallites are formed by linear chains of clusters consisting of defects. The number of particles in the system is $N = 10^6$.

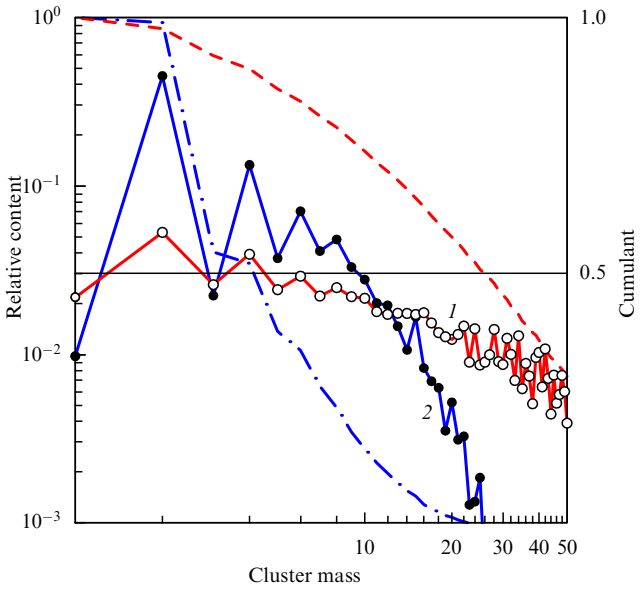

Figure 8. (Color online.) Distribution $W_c(N)$ of structural defect clusters by mass (the number N of defects in a cluster) for a melted (solid red line, *1*) and crystallizing (solid blue line, *2*) Yukawa system. Cumulative distributions C_W of these spectra ($C_W(N) = \sum_N^\infty W_c$) are shown by the red dashed and blue dot-and-dash lines, respectively. Note the strong difference between the two distributions; in particular, half of the defects for the liquid phase concentrate in clusters with $N_h < 25$ (where N_h is determined from the relation $C_W(N_h) = 0.5$), whereas $N_h < 5$ for the solid phase. In both cases, pair defects (dislocations) prevail in the system.

the system should be sufficiently large, $N \gg 10^4$, which is far beyond what can be achieved in current CP experiments ($N_{exp} \simeq 10^4$). The distribution of crystallites by size or by the number of constituent particles can be used as an order parameter characterizing the melting and crystallization of two-dimensional systems; clearly, the size of a crystallite in a liquid phase tends to zero.

Another important parameter characterizing the phase state of a two-dimensional Yukawa system is the distribution of clusters, $W_c(N)$, by the number N of defects they contain (or the mass distribution of defect clusters). Here, $W_c(N)$ is defined such that $\sum_1^\infty W_c = 1$. Figure 8 presents such distributions both for a melted and crystallizing two-dimensional CP. Note the considerable difference between the two distributions: the liquid phase shows a shallow decrease in $W_c(N)$ for large N, indicating the presence of large ($N > 100$) clusters in the system, whereas for the solid phase, clusters with $N > 30$ are virtually absent.

In both cases, the size distribution of defects is a zigzag-like and dominated by dislocations (5–7 defects with $N = 2$). The cumulative distributions $C_W(N)$ ($C_W(N) = \sum_N^\infty W_c$) for the spectra are shown in Fig. 8. One clearly sees a difference between these cumulative distributions; in particular, half of defects for the liquid phase concentrate in clusters with $N_h < 25$ ($C_W(N_h) = 0.5$), whereas $N_h < 5$ for the solid phase. The region of the crystal–liquid phase transition exhibits a sharp increase in the parameter N_h. Thus, the cumulants of the defect mass distribution can also be used as order parameters for describing the melting of a two-dimensional CP.

In considering the mass (or size) distribution of clusters, it is natural to take a look at their shape. Figure 9 gives typical examples of clusters for a melted (a) and a crystallizing (b) Yukawa system. Introducing the fractal cluster dimensionality F: $N(r) \propto r^F$, where $N(r)$ is the number of point defects in a cluster in a sphere of radius r ($r = 0$ at the cluster's center of mass), it is clearly seen that these clusters are totally different in the fractal dimension: $F \simeq 1.5-1.7$ (depending on the cluster mass N) for the liquid phase, and $F \approx 1$ for the crystallizing system. Thus, such a metrics as the fractal dimension of clusters consisting of defects can serve as an order parameter to characterize the melting of a two-dimensional Yukawa system. It is evident that the value of F experiences a jump in the region of the crystal–liquid phase transition.

A further major characteristic of a phase state is the displacement of the ith microparticle, $\delta r_i^2(t_0, \tau)$, relative to its initial position $\mathbf{r}_i(t_0)$, defined as

$$\delta r_i^2(t_0, \tau) = \left[\mathbf{r}_i(\tau + t_0) - \mathbf{r}_i(t_0)\right]^2 . \qquad (15)$$

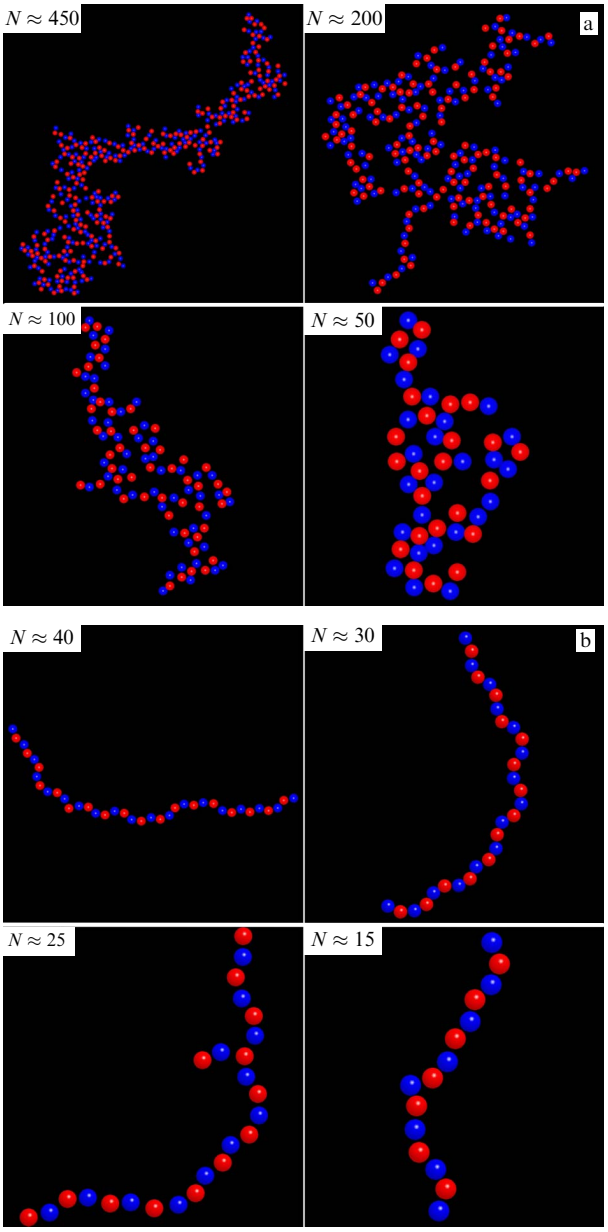

Figure 9. (Color online.) Typical examples of point defect clusters (the number of defects N for each cluster is given in the upper left corner) for a melted (a) and crystallizing (b) two-dimensional Yukawa system. Colors of microparticles in a cluster: red (black) for particles with 7 or more nearest neighbors (NN), and blue (gray/white) for particles with 5 or fewer NN. Melt exhibits a complex fractal structure of clusters; for the solid phase, clusters consist primarily of linear chains of defects. This makes it possible to use cluster shape in constructing an order parameter characterizing the melting of two-dimensional systems.

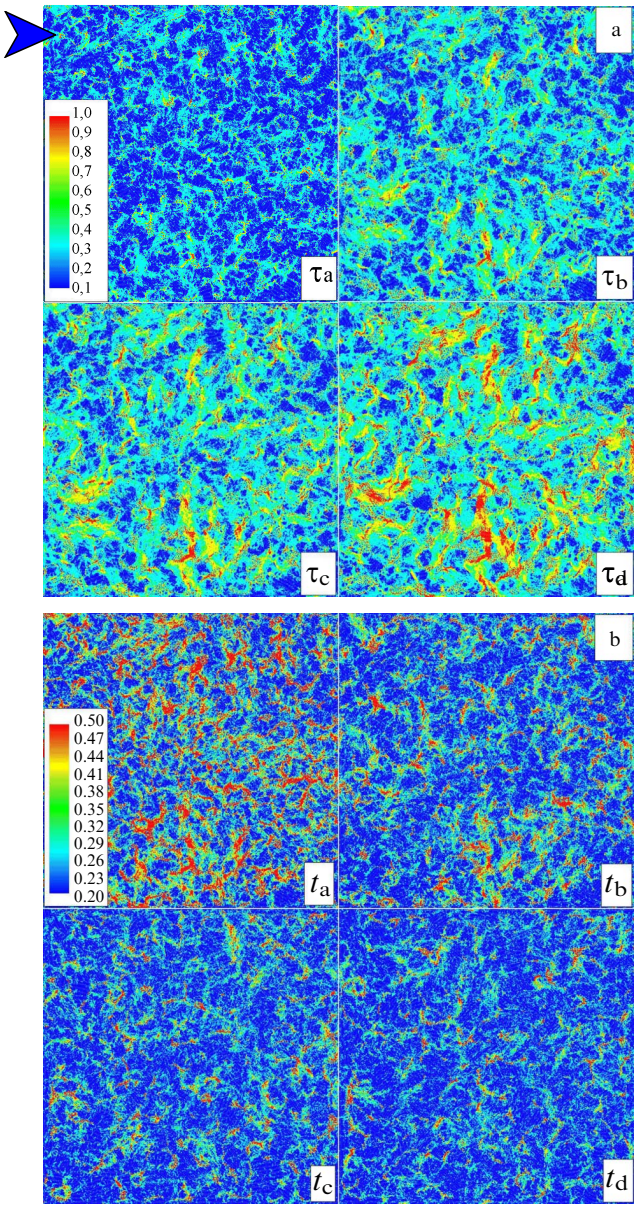

Figure 10. (Color online.) Displacement field $\delta r_i^2(t,\tau)$ (normalized to the interparticle distance) for a crystallizing Yukawa system. Evolution of the displacement field: (a) at different instances of time τ ($\tau_a < \tau_b < \tau_c < \tau_d$) for fixed t; (b) at different crystallization stages t ($t_a < t_b < t_c < t_d$) of the system (for a fixed value of the parameter τ). Clearly seen is the appearance of spatial structures (the motion of microparticles occurs primarily near defects), which is qualitatively different from a similar picture for a melted system, where the displacement field is by far more uniform.

For two-dimensional systems, it is known that such a displacement, when averaged over all the particles, increases with time for both liquid and solid phases. Mention can also be made of the proposal in Ref. [11] of applying a modified Lindemann criterion which takes into account the average runaway of the neighboring particles with time; the rate of this runaway is markedly different between the liquid and solid phases. Here, rather than dwelling on these average characteristics, we shall consider the field of displacements $\delta r_i^2(t,\tau)$ and its properties.

Displacement fields characteristic of a crystallizing Yukawa system are demonstrated in Fig. 10. Panel (a) shows the evolution of the displacement field on different time scales, and panel (b) depicts it for different crystallization stages (for a specified value of the parameter τ). The appearance of spatial structures indicates that the motion of microparticles mostly occurs near defects, which is in qualitative contrast to the similar situation for a melted system, when the displacement field is much more uniform. [7] Note that, in spite of the high mobility of defects in such a

[7] To make things more visual, the evolution of the displacement field on various time scales is also presented in a computer animated form in this paper's online version at www.ufn.ru.

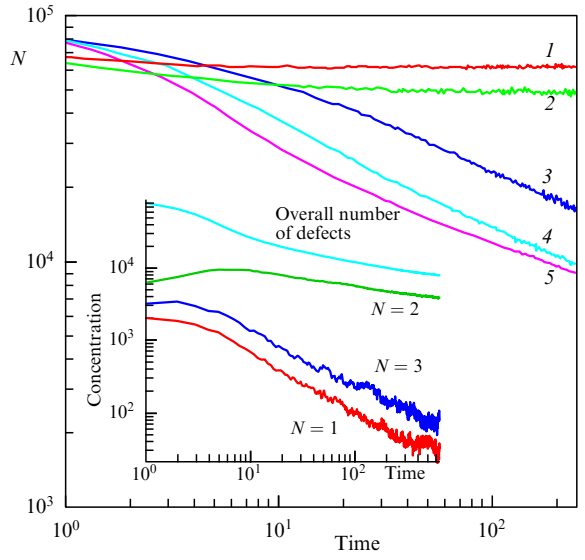

Figure 11. (Color online.) Time dependence of the number of point defects in a two-dimensional Yukawa system for different microparticle temperatures T_d: T_d decreases from red (*1*) to purple (*5*). Inset displays how clusters of defects of different masses disappear in a crystallizing Yukawa system (the time evolution of disclinations ($N = 1$), dislocations ($N = 2$), and clusters with $N = 3$ is shown).

system, they have virtually the same temperature as most of the microparticles with 6 neighbors. This result was obtained by the MD simulation of a crystallizing Yukawa system (with $N = 10^6$) without considering friction, so as to exclude effects due to the Langevin thermostat.

The discussion above considers some order parameters that characterize the melting and crystallization of a two-dimensional CP and which have a relation to the properties of structural defects. Let us now consider in more detail the kinetics of defects, which is a factor of extreme importance in the physics of melting and crystallization. It has already been shown above that the region near the crystal–liquid phase transition in a Yukawa system is dominated by the presence of pair defects, i.e., relatively stable pairs of defects consisting of particles with 5 and 7 nearest neighbors.[***]

The description of the interaction between these pair defects is one of the major problems yet to be solved. MD simulations (see web version of the paper for animation) clearly reveal strong attraction between pair defects and show that the result of this interaction depends on the mutual orientation of the interacting defects, thus demonstrating either annihilation (recombination) at their one orientation or the formation of a cluster of four defects, usually a linear 5–7–5–7 one.

Figure 11 depicts how the total concentration of defects varies with time at different microparticle temperatures T_d in a two-dimensional CP. Note the important result that, above the threshold temperature (a certain T_m, which can naturally be related to the melting point), the defect concentration in the system settles down rather quickly. The size distribution of defect clusters and other order parameters discussed above can be shown as well to settle down.

[***] As thorough analysis shows defect clusters with mass 4 are dominant in the defect cluster mass distribution (see Ref. [54]). (*Author's note added in English proof.*)

For $T_d < T_m$, the characteristic time τ_{eq} for coming the system to equilibrium (in defect concentration) dramatically increases, as Fig. 11 clearly shows. It is for this reason especially that the calculations presented here failed to reach the quasistationary defect concentrations for $T_d < T_m$. It should be added that, as shown in the inset to Fig. 11, defects of different masses annihilate at different rates: disclinations ($N = 1$) and clusters of three point defects ($N = 3$) recombine much faster than dislocations ($N = 2$).

This means, in particular, that the distribution of defects in a crystallizing Yukawa system changes with time. The time τ_{eq} required for the establishment of equilibrium in the system increases dramatically with decreasing temperature T_d (or increasing the coupling parameter Γ), so that already in the prethreshold region a situation may readily occur in which this time is much larger than the characteristic duration of an experiment. Lowering the temperature still further drastically decreases the defect mobility and gives rise to the effect of defect quenching, when the defect concentration is super-equilibrium and changes very slowly with time. Therefore, virtually all experiments with two-dimensional plasma crystals in CP utilize a nonequilibrium crystallizing plasma as their object of study. Therefore, the kinetics of defects yield one more important order parameter, viz. the characteristic time τ_{eq}. Note also that another possible choice for an order parameter are various metrics of the mass distribution $W_c(N)$ of clusters, for example, the parameters $W_c(2)/W_c(4)$ or $W_c(2)/W_c(1)$, etc.

Figure 12 illustrates how metrics characterizing local and orientational orders change at different Γ. Shown are the relative density N_6/N of microparticles with 6 neighbors (red dots) and the cumulant of the distribution of microparticles over the parameter $|\Psi_6|$. The inset depicts the distributions Ψ_6 for the melt (blue solid line) and for the plasma crystal (orange solid line); the crystalline phase characteristically features two

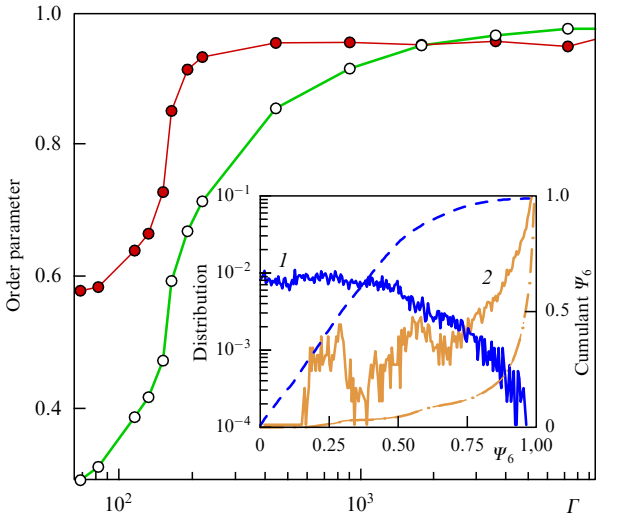

Figure 12. (Color online.) Order parameters versus coupling parameter Γ for a two-dimensional Yukawa system. Presented are a local order characteristic, the relative density N_6/N of microparticles with 6 neighbors (red dots), and a characteristic of short-range orientational order, the cumulant of the distribution of function Ψ_6 (white dots). Insert: the distributions Ψ_6 for melt (blue line *1*) and for crystal (orange line *2*). The cumulants of these distributions are shown by a red dashed line and an orange dash-and-dot line, respectively. A clear feature is the sharp decrease in order parameters (melting) for $\Gamma < \Gamma_m \sim 150$ (which corresponds to the microparticle temperature $T_m \simeq 6000$ K).

peaks, due to the presence of point defects with 5 and 7 nearest neighbors. The cumulants of these distributions are shown by a dashed line of the same color. One observes a sharp decrease in order parameters (the melting of the system) for $\Gamma < \Gamma_m \sim 150$ (corresponding to the microparticle temperature $T_m \simeq 6000$ K). It is seen that the orientational order parameter is by far more sensitive to a change in Γ than the parameter N_6/N. It is readily shown that the change $\delta\langle\Psi_6\rangle \propto \delta T_d$ in the region of $\Gamma \sim 10^3$, where the local order parameter virtually does not change. Note that, because these order parameters are nonequilibrium for $\Gamma > \Gamma_m$, their values were calculated using one and the same relaxation time for a Yukawa system assumed to have the same initial superequilibrium distribution of defects in 2D space. At still higher values of Γ, the above-described quenching effect shows itself, which causes the order parameter values to decrease with increasing Γ. The change with time in the concentration of structural defects in a two-dimensional CP can be described using the balance equation

$$\frac{\partial n_d}{\partial t} = q_d - \alpha_d n_d^2 , \qquad (16)$$

where n_d is the concentration of point defects in the system, whose creation and annihilation are described by the terms q_d, $\alpha_d n_d^2$. As already noted, defects of various masses annihilate at different rates in a crystallizing CP; however, because the clusterization of defects in such a system has been more or less understood, this simple description of defect kinetics may be highly productive. Equation (16) assumes, for simplicity, that defects annihilate in pair collisions and so neglects, for example, multiparticle collision processes. In the phase transition region, which is of particular interest in this study, the defect concentration is not very high, the loss of defects is primarily determined by annihilation of pair defects (dislocations), and hence this assumption is valid. In the quasi-equilibrium state, the defect concentration is given by $n_d^2 = q_d/\alpha_d$.

Figure 13 plots the square of the defect concentration, n_d^2, in a two-dimensional CP as a function of the microparticle temperature in the crystal–liquid phase transition region. The

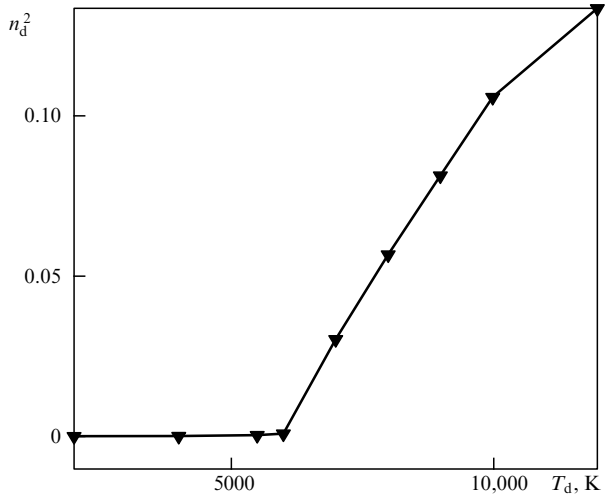

Figure 13. Square of the defect concentration, n_d^2, versus microparticle temperature T_d for a two-dimensional Yukawa system. The kink is close to the region of the crystal–liquid phase transition; the transition temperature $T_m \simeq 6000$ K, corresponding to $\Gamma \sim 150$.

first point to note is the linear increase in the parameter n_d^2 in the above-threshold region (for $T_d > T_m$, where the defect concentration rapidly becomes equilibrium), pointing to an important link between the defect creation and annihilation rates: $n_d^2 = q_d/\alpha_d \propto (T_d - T_m)$. In the subthreshold region, for a microparticle temperature $T_d < T_m$, the parameter q_d/α_d decreases dramatically and, as noted above, the characteristic time for the defect concentration to come to a quasi-equilibrium level sharply increases. The defect annihilation rate, as seen from Fig. 11, does not change very strongly in the transition region, resulting in a sharply decreased defect creation rate q_d. The parameters q_d and n_d^2 can also be used as order parameters characterizing the melting of a two-dimensional CP. In Fig. 13, the defect concentration shows a clear kink at microparticle temperature $T_m \simeq 6000$ K (for which the corresponding coupling parameter is $\Gamma_m \simeq 150$). As with order parameters (see Fig. 12), the (nonequilibrium) defect concentration for $T < T_m$ was calculated for one and the same CP relaxation time, and one and the same initial spatial defect distribution. Quasi-equilibrium defect concentrations for $T < T_m$ were not achieved because of excessive computer time requirements, so those values of n_d^2 shown in Fig. 13 are superequilibrium. Note that the kink observed in the behavior of n_d^2 at $T = T_m$ implies that the melting of two-dimensional CP is a second-order phase transition.

4. Conclusions

The melting and crystallization aspects of CP considered in this article make it possible to suggest new order parameters characterizing the solid–liquid phase transition and to derive new melting criteria for such systems.

In the case of a three-dimensional CP, both the experiments recently performed aboard the ISS and the numerical simulation of the Yukawa system, which describes in a simplified way the interaction between microparticles in a CP, make it possible to introduce such order parameters. Melting and premelting parameters for a three-dimensional CP can, as shown here, be derived from local order parameters, specifically the distribution of dusty microparticles over the values of rotational invariants of various ranks. The cumulants of these distributions are highly sensitive to the phase state of a CP and therefore enable the description of the crystal–liquid phase transition. Using such cumulants, it is easy to determine the presence in a system of even small fractions of various crystal lattice types. For example, the space experiments discussed above observed the premelting of a plasma crystal, i.e., the gradual disappearance of small solid-state fractions, fcc and bcc clusters, from the system. An important point to note is that, unlike their dynamic (Lindemann-like) counterparts, the melting criteria we proposed for a three-dimensional CP require no knowledge of particle trajectories: a few snapshots of a system suffice to determine its phase state.

The melting and crystallization of a two-dimensional CP were also addressed by considering the example of the evolution of a confined Yukawa system for different microparticle temperatures. A two-dimensional CP undergoing a crystal–liquid phase transition is specific in that, in order to find the order parameters describing this transition, it is necessary to study the behavior of relatively large systems with a number of particles $N > 10^6$, which, to date, can be done only numerically, by using MD methods (unfortunately, today's experiments with complex and colloidal plasmas are

lagging two orders of magnitude behind in their capabilities (see, for example, Ref. [50]). Such numerical experiments were performed and a detailed study was made of the kinetics of defects in a two-dimensional CP close to the crystal–liquid phase transition region. Important order parameters describing the melting and crystallization of two- and quasi-two-dimensional systems were found. Among these are the distribution of defect clusters by size (mass), which changes dramatically in the phase transition region, and its derivatives. Another major order parameter is the shape of a cluster consisting of defects; it is shown that the fractal dimension of such clusters changes sharply at the phase transition point. Specific features of defect kinetics at various microparticle temperatures also enable the introduction of a number of new order parameters, such as the defect concentration and the characteristic time for defects to reach their quasi-equilibrium concentration, a time which changes sharply in the phase transition region. This usually results in experimentally examined two-dimensional plasma crystals becoming strongly nonequilibrium; in particular, spatial correlations (for example, those of orientational order Ψ_6) in a system of microparticles become nonstationary. It is therefore logical to call such system crystallizing rather than crystallized.

It is hoped that the proposed order parameters greatly extend our understanding of the crystal–liquid phase transitions. Notice that the applicability of the proposed criteria is not necessarily limited to complex plasma but can be extended to virtually any system close to the solid–liquid phase transition.

Acknowledgments. Gratitude for interest and useful discussions goes to all those who participated in the April 6, 2010 session of the Seminar on Solid State Physics of the I E Tamm Theoretical Physics Department at the P N Lebedev Physics Institute, RAS. Special thanks are due to E G Maksimov and S M Apenko, whose remarks and suggestions were helpful in improving this work.

References

1. Fortov V E et al. *Usp. Fiz. Nauk* **174** 495 (2004) [*Phys. Usp.* **47** 447 (2004)]
2. Morfill G E et al. *Contrib. Plasma Phys.* **44** 450 (2004)
3. Morfill G E et al. *Phys. Scripta* **T107** 59 (2004)
4. Robbins M O, Kremer K, Grest G S *J. Chem. Phys.* **88** 3286 (1988)
5. Morfill G E et al. *Phys. Rev. Lett.* **92** 175004 (2004)
6. Rubin-Zuzic M et al. *Nature Phys.* **2** 181 (2006)
7. Klumov B A, Rubin-Zuzic M, Morfill G E *Pis'ma Zh. Eksp. Teor.* **84** 636 (2006) [*JETP Lett.* **84** 542 (2006)]
8. Zuzic M et al. *Phys. Rev. Lett.* **85** 4064 (2000)
9. Arp O et al. *Phys. Rev. Lett.* **93** 165004 (2004)
10. Mitic S et al. *Phys. Rev. Lett.* **101** 125002 (2008)
11. Bedanov V M, Gadiyak G V, Lozovik Yu E *Phys. Lett. A* **109** 289 (1985)
12. Zahn K, Maret G *Phys. Rev. Lett.* **85** 3656 (2000)
13. Chu J H, Lin I *Phys. Rev. Lett.* **72** 4009 (1994)
14. Thomas H et al. *Phys. Rev. Lett.* **73** 652 (1994)
15. Ikezi H *Phys. Fluids* **29** 1764 (1986)
16. Konopka U, Morfill G E, Ratke L *Phys. Rev. Lett.* **84** 891 (2000)
17. Ivlev A V et al. *Phys. Rev. Lett.* **100** 095003 (2008)
18. Klumov B et al. *Plasma Phys. Control. Fusion* **51** 124028 (2009)
19. Klumov B A et al. *Eur. Phys. Lett.* **92** 15003 (2010)
20. Raveché H J, Mountain R D, Streett W B *J. Chem. Phys.* **61** 1970 (1974)
21. Steinhardt P J, Nelson D R, Ronchetti M *Phys. Rev. B* **28** 784 (1983)
22. Auer S, Frenkel D *J. Chem. Phys.* **120** 3015 (2004)
23. Klumov B A, Morfill G E *Pis'ma Zh. Eksp. Teor. Fiz.* **87** 477 (2008); *Zh. Eksp. Teor. Fiz.* **134** 1059 (2008) [*JETP Lett.* **87** 409 (2008); *JETP* **107** 908 (2008)]
24. Berezinskii V L *Zh. Eksp. Teor. Fiz.* **59** 907 (1970) [*JETP* **32** 493 (1971)]
25. Kosterlitz J M, Thouless D J *J. Phys. C: Solid State Phys.* **6** 1181 (1973)
26. Nelson D R, Halperin B I *Phys. Rev. B* **19** 2457 (1979)
27. Young A P *Phys. Rev. B* **19** 1855 (1979)
28. Pitaevskii L P *Usp. Fiz. Nauk* **176** 345 (2006) [*Phys. Usp.* **49** 333 (2006)]
29. Lewenstein M et al. *Adv. Phys.* **56** 243 (2007)
30. Geim A K, Novoselov K S *Nature Mater.* **6** 183 (2007)
31. Morozov S V, Novoselov K S, Geim A K *Usp. Fiz. Nauk* **178** 776 (2008) [*Phys. Usp.* **51** 744 (2008)]
32. Guillamón I et al. *Nature Phys.* **5** 651 (2009)
33. Gasser U *J. Phys. Condens. Matter* **21** (20) 203101 (2009)
34. Bowick M J, Giomi L *Adv. Phys.* **58** (5) 449 (2009)
35. Lipowsky P et al. *Nature Mater.* **4** 407 (2005)
36. Shukla P K, Eliasson B *Rev. Mod. Phys.* **81** 25 (2009)
37. Pertsinidis A, Ling X S *Nature* **413** 147 (2001)
38. Thomas H M, Morfill G E *Nature* **379** 806 (1996)
39. Chu J H, Lin I *Phys. Rev. Lett.* **72** 4009 (1994)
40. Woon W-Y, Lin I *Phys. Rev. Lett.* **92** 065003 (2004)
41. Hartmann P et al. *Phys. Rev. E* **72** 026409 (2005)
42. Naidoo K J, Schnitker J *J. Chem. Phys.* **100** 3114 (1994)
43. Qi W-K et al. *J. Phys. Condens. Matter* **20** 245102 (2008)
44. Reichhardt C, Reichhardt C J O *Phys. Rev. Lett.* **90** 095504 (2003)
45. Couëdel L et al. *Phys. Rev. Lett.* **103** 215001 (2009)
46. Klumov B A, Morfill G E *Pis'ma Zh. Eksp. Teor. Fiz.* **90** 489 (2009) [*JETP Lett.* **90** 444 (2009)]
47. Frenkel D, Smit B *Understanding Molecular Simulation: from Algorithms to Applications* (San Diego: Academic Press, 2002)
48. Klumov B A, Morfill G E *Pis'ma Zh. Eksp. Teor. Fiz.* **85** 604 (2007) [*JETP Lett.* **85** 498 (2007)]
49. Somer F L (Jr.) et al. *Phys. Rev. Lett.* **79** 3431 (1997)
50. Knapek C A et al. *Phys. Rev. Lett.* **98** 015004 (2007)
51. Ryzhov V N *Zh. Eksp. Teor. Fiz.* **100** 1627 (1991) [*Sov. Phys. JETP.* **73** 899 (1991)]
52. Ryzhov V N, Tareeva E E *Phys. Rev. B* **51** 8789 (1995)
53. Ryzhov V N et al. *Usp. Fiz. Nauk* **178** 1118 (2008) [*Phys. Usp.* **51** 1077 (2008)]
54. Klumov B A *Eur. Phys. Lett.* (2011) (submitted)